Int. J. Heat Mass Transfer. Vol. 21, pp. 935–945

0017-9310/78/0701-0935 $02.00/0

NUMERICAL PREDICTION OF HEAT-TRANSFER CHARACTERISTICS OF FULLY DEVELOPED LAMINAR FLOW THROUGH A CIRCULAR CHANNEL CONTAINING ROD CLUSTERS

R. W. BENODEKAR* and A. W. DATE†
Department of Mechanical Engineering, Indian Institute of Technology, Powai, Bombay 400 076, India

(*Received* 1 *April* 1977 *and in revised form* 6 *December* 1977)

Abstract—This paper presents the results of computations for a fully developed laminar flow in rod cluster assemblies. The problem is solved by a finite difference method using a sector approach, where only the smallest symmetry segment of the cluster is considered to be the characteristic flow area. The pressure drop characteristics are reported in terms of friction factor Reynolds number products and are compared with those available in the literature. Nusselt numbers are presented for several configurations. The results are expressed as functions of channel wall spacing, radial displacement of the rod rings, the number of rods in the assembly and rod diameters.

NOMENCLATURE

b_1, b_2, b_3, radii of the peripheral rod rings nondimensionalised with respect to R_c;
D, rod diameter;
D_h, hydraulic diameter based on wetted perimeter, $D_h = \dfrac{4 \times \text{flow area}}{\text{wetted perimeter}}$;
D_{h_1}, hydraulic diameter based on heated perimeter, $D_{h_1} = \dfrac{4 \times \text{flow area}}{\text{heated perimeter}}$;
d_h, d_{h_1}, hydraulic diameter parameters nondimensionalised with respect to R_c;
f, Fanning friction factor;
h, heat-transfer coefficient;
h_1, h_2, d, e, directional distances (see Fig. 2);
k, thermal conductivity of the fluid;
Nu, Nusselt number, $Nu = hD_h/k$;
N_r, N_t, number of radial and tangential grid lines respectively;
P, pitch distance between rods non-dimensionalised with respect to R_c, (see Fig. 10);
dP/dz, axial pressure gradient;
q, axially and peripherally uniform heat flux at the rod surface;
R, dimensional radius;
R_c, channel radius;
Re, Reynolds number, $Re = \rho \bar{u} D_h/\mu$;
r_0, r_1, r_2, r_3, rod radii non-dimensionalised with respect to R_c;
r, θ, z, cylindrical coordinates;
T, temperature;
T^*, nondimensional temperature defined by equation (5);
$\bar{T}_f$, bulk mean temperature of fluid;
$\bar{T}_w$, average temperature of heated perimeters;
$\bar{T}_{w_0}$, average temperature of central rod;
$\bar{T}_{w_1}, \bar{T}_{w_2}, \bar{T}_{w_3}$, average temperatures of peripheral rods;
$\bar{T}_{w_c}$, average temperature of channel wall;
$\partial T/\partial n$, normal gradient temperature;
u, axial velocity;
u^*, nondimensional axial velocity defined by equation (2);
$\bar{u}$, average velocity;
W, wall spacing; distance between the channel wall and outermost rod ring (e.g. in case of 3 rod ring cluster, $W = 1 - b_3$) nondimensionalised with respect to R_c.

Greek symbols

ε, eccentricity, $\varepsilon = b_1/(1 - r_0)$;
ϕ, angle of the symmetry sector;
ρ, density of the fluid;
μ, viscosity of the fluid;
ψ, angle between the line of intersection and the normal to the boundary (see Fig. 2).

Subscripts

i, number of rod ring;
0, central rod.

Other notation

$F\{\ \}$, function of.

*Senior research fellow.
†Assistant professor.

1. INTRODUCTION

THE ROD cluster assembly consisting of parallel arrays of fuel rods inside a circular channel has become a principal configuration of the nuclear reactor core. The problem of predicting the characteristics of the in-line flow of a cooling medium in these configurations is complicated by its turbulent nature and the complex geometry. Although the flow is mostly turbulent the laminar flow results provide upper bound to the rod temperatures and lower bound to the Nusselt numbers. The laminar flow results are also directly applicable to the low velocity regions that could occur due to fault conditions.

The heat-transfer problem of a flow through a rod cluster assembly is quite difficult to solve analytically or numerically. The complexities introduced by non-orthogonal intersections of the boundaries with the grid lines and the Neumann boundary conditions specified at the boundaries make the problem analytically intractable. Nonetheless, a few analytical solutions are available for constant temperature boundary condition around the rod surface with simplified geometry such as infinite rod arrays. The velocity and temperature solutions for this problem have been obtained by Sparrow *et al.* [1, 2]. The infinite rod array problem with specified constant heat flux around the rod surface has also been solved numerically by Dwyer and Berry [3].

The analytical solutions for finite rod bundles are limited to the prediction of fluid flow characteristics only. The single rod ring cluster problem has been analysed by Min *et al.* [4] and they have presented results in the form of velocity profiles and friction factor–Reynolds number products. Axford [5] has solved the problem analytically and has presented some velocity profiles. Zarling [6] has further analysed the same problem more accurately and provided results of $f \cdot Re$ products as a function of a number of geometrical parameters. The analytical solutions to the fluid flow problem of multiple rod ring clusters with arbitrary rod arrangements have been obtained by Mottaghian and Wolf [7].

It may be noted that, although, the analytical solutions in principle are applied to a continuum, it has been necessary in methods used by some of the above authors [1, 2, 4] to restrict satisfaction of the boundary conditions to a discrete number of points suitably chosen on the boundary.

A finite difference technique has also been used to solve the rod cluster problem. Gunn and Darling [8] attempted to calculate fluid flow characteristics in a finite 4-rod bundle for the first time. Rehme [9] followed the same approach for the solution of a 7-rod cluster. However, he has reported that the solution for bundles with more than seven rods resulted in an enormous consumption of computer time and storage. Therefore, he proposed a subchannel approach based on the superposition of the local subcell solutions. Although the subchannel analysis simplifies the numerical solution procedure it requires prior knowledge of various characteristics for different subcells and introduces fictitious quantities such as subchannel mixing in the calculations.

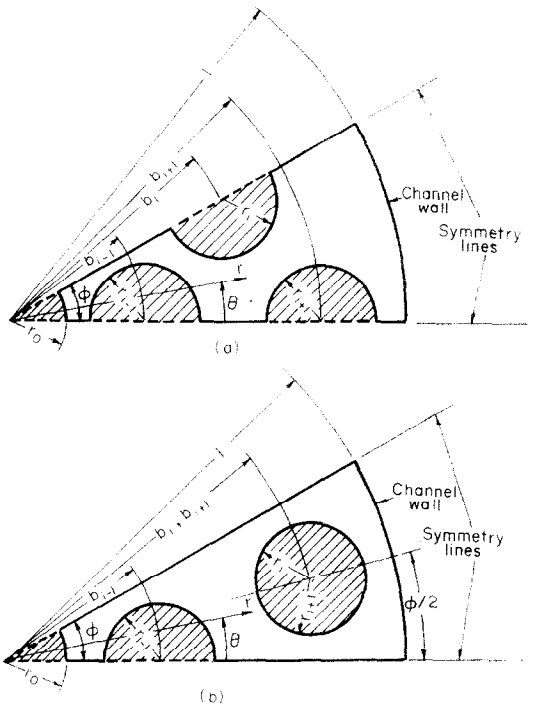

FIG. 1. Symmetry sectors of a rod cluster assembly. (a) Singly connected; (b) Doubly connected.

Under the present investigation the problem has been solved by a finite difference method using the sector approach where the smallest symmetry segment is considered to be the characteristic flow area. Such sectors for singly and doubly connected assemblies are shown in Fig. 1. In this figure an arbitrary number of half rods with radii $r_i (i = 1, 2, 3 \ldots)$ placed on concentric rings of radii b_i around a central rod with radius r_0 are shown. The present method of solution solves the basic equations of momentum and energy over the symmetry sector, thereby eliminating the need for any empirical input like, for example, information on subchannel mixing. The difficulties encountered by Rehme [9] in applying overall numerical procedures to rod clusters with more than seven rods have been overcome in the present work by incorporating efficient treatment of boundary conditions and using a fast converging iterative method. The problem of heat transfer in the most complex geometry solved by the present method required 55 s of CPU time and 15 K storage on a DEC system 10 computer.

2. FORMULATION OF THE PROBLEM AND METHOD OF SOLUTION

2.1. *The mathematical problem*

The fully developed, laminar, incompressible, constant property axial flow is governed by the following dimensionless momentum equation in cylindrical coordinates:

$$\frac{1}{r}\frac{\partial}{\partial r}\left(r\frac{\partial u^*}{\partial r}\right)+\frac{1}{r^2}\frac{\partial^2 u^*}{\partial \theta^2} = -1. \qquad (1)$$

The dimensionless velocity and the radial coordinate in the above equation are defined as

$$u^* = \frac{u}{\frac{1}{\mu}\left(-\frac{dP}{dz}\right)R_c^2}, \tag{2}$$

$$r = \frac{R}{R_c}. \tag{3}$$

The boundary conditions for the momentum equation are:

(i) $u^* = 0$ on all rod surfaces and on the channel wall (see Fig. 1), and

(ii) $\frac{\partial u^*}{\partial \theta} = 0$ on the lines of symmetry.

The fully developed temperature field is governed by the dimensionless energy equation in cylindrical coordinates as

$$\frac{1}{r}\frac{\partial}{\partial r}\left(r\frac{\partial T^*}{\partial r}\right)+\frac{1}{r^2}\frac{\partial^2 T^*}{\partial \theta^2} = \frac{4}{d_h d_{h_1}}\frac{u}{\bar{u}}; \tag{4}$$

where the dimensionless temperature is given by

$$T^* = \frac{T - T_{\min}}{qD_h/k}. \tag{5}$$

The dimensionless temperature, T^* is defined here with respect to the minimum temperature in the flow field so that in a thermal entry length situation, for example, the minimum temperature, $T_{\min}$ will equal the uniform inlet temperature when the temperature profile has just reached the fully-developed condition.

The boundary conditions for the energy equation are:

(i) axially constant heat flux on the rod surfaces;
(ii) peripherally uniform and equal heat fluxes on all the rods;
(iii) zero heat flux on the channel wall and
(iv) zero heat flux on the lines of symmetry.

These boundary conditions are no doubt idealisations; for the heat fluxes are not axially or even peripherally uniform, nor are the heat fluxes equal at all rods. These idealisations, however, allow prediction of the heat-transfer situation by a simple two-dimensional Poisson equation (4). The assumption of axially uniform heat flux is necessary for consideration of the thermally fully-developed profile, whereas peripheral uniformity of heat flux is considered to ensure sectoral symmetry of the temperature profile. The assumption of zero heat flux on the channel wall is introduced to indicate the fact that heat loss through the channel wall is indeed very small compared to the heat flux delivered by the rods.

2.2. *Method of solution*

A grid consisting of radial and tangential lines is set up over the symmetry sector of the rod cluster assembly. Differential equations (1) and (4) are written in finite difference (f.d.) forms and they are solved for the interior nodes using the Alternating Direction Implicit (ADI) iterative technique [10].

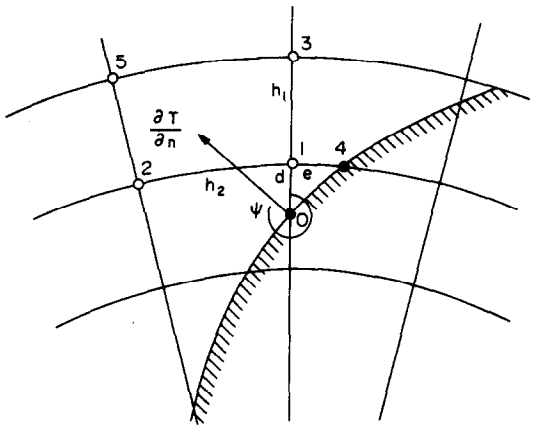

FIG. 2. A typical irregular intersection of the grid lines with the boundary.

For the near-wall nodes the values of the variables at the grid intersections with the boundary (see, for example, points 0 and 4 as shown in Fig. 2) are involved in the finite difference equations. Since the velocities at the solid walls are known, the f.d. equations for velocity are solved only at the interior nodes. However, in the heat-transfer problem for which Neumann boundary conditions are specified at the boundaries, it is necessary to solve for the boundary point temperatures separately in addition to the interior grid nodes. The main task then is to express the Neumann condition in a finite difference form. The method for treating the boundary condition is given by Greenspan [11]; in the present work a variant of his method is used [15].

2.3. *Accuracy and measure of convergence*

The numerical accuracy of the solution has been tested by confirming the grid independence of the solutions. For example, for the symmetry sector of a

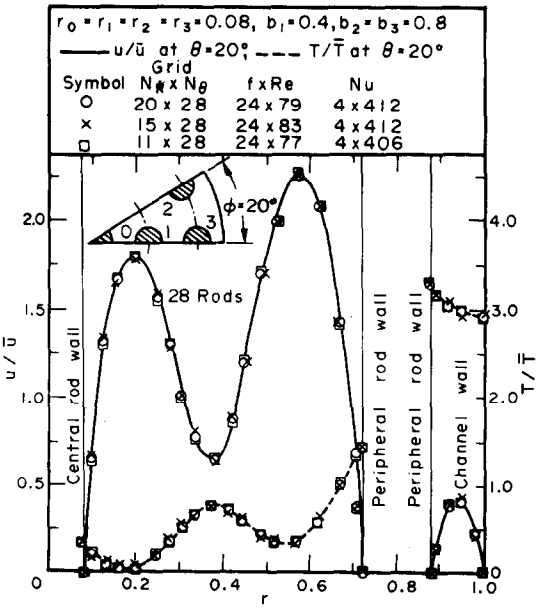

FIG. 3. Effect of the grid size on the velocity and temperature profiles on the symmetry line.

28-rod cluster, three different mesh sizes were used. Figure 3 shows the predicted velocity and temperature profiles at $\theta = 20°$ (i.e. the upper line of symmetry). Included in the figure are also the overall characteristics $f \cdot Re$ and Nu. As can be seen that for the grid dispositions the variance in the predictions is negligible. From the calculations it was found that for 11 $\times$ 28 grid the average error in $u/\bar{u}$ value as compared to 20 $\times$ 28 grid was 0.2% and the average error in $T/\bar{T}$ was 0.5% (percentage error was based on the local value).

The convergence of the solution was tested by fractional change as well as the residual source criterion; the latter is estimated by calculating the imbalance in the f.d. equation for the interior nodes. This, unlike the former, is insensitive to the number of grid lines.

3. RESULT AND DISCUSSION

3.1. *Introduction*

The fluid flow (i.e. product $f \cdot Re$) and the heat-transfer (i.e. Nu) characteristics for a fully developed laminar flow depend only on the geometrical parameters when the secondary flows are absent. Such being the present case, the functional dependence of $f \cdot Re$ is written as:

$$f \cdot Re = F\{r_0, r_i, b_i, W, \phi\}, \tag{6}$$

where

$$f = \frac{\left(-\frac{dP}{dz}\right) D_h}{2\rho \bar{u}^2}. \tag{7}$$

Using the Reynolds number based on the hydraulic diameter, D_h and the definition of dimensionless velocity from equation (2), the $f \cdot Re$ product is obtained as

$$f \cdot Re = \frac{d_h^2}{2\bar{u}^{*2}}, \tag{8}$$

where

$$\bar{u}^* = \frac{\iint u^* r \, dr \, d\theta}{\iint r \, dr \, d\theta}. \tag{9}$$

The average heat-transfer coefficient h is defined as

$$h = \frac{q}{T_w - T_f}. \tag{10}$$

Hence the Nusselt number based on D_h using the definition of dimensionless temperature given by equation (5) can be written as

$$Nu = \frac{1}{T_w^* - T_f^*}, \tag{11}$$

where

$$T_f^* = \frac{\iint T^* u^* r \, dr \, d\theta}{\iint u^* r \, dr \, d\theta}, \tag{12}$$

and

$$T_w^* = \frac{\int T_w^* \, ds}{\int ds}, \tag{13}$$

where ds is the incremental length along the solid heated boundaries. The integrals in equations (8), (12) and (13) were evaluated by Simpson's rule.

The functional dependence of Nu on the geometrical parameters is presented as

$$Nu = F\{r_0, r_i, b_i, W, \phi\}. \tag{14}$$

3.2. *Confirmatory results*

In order to check the validity of the present method and the computer program, the following cases for which heat-transfer solutions are available were solved.

Case 1. Laminar fully developed flow heat transfer in an annulus with radius ratio, $R_0/R_c = 0.2$ with inner cylinder at uniform heat flux and outer wall insulated [12].

Case 2. Laminar fully developed flow heat transfer in a uniform heat flux equilateral triangular infinite rod array with $P/D = 1.6$ and 2.0 [3].

The results for the above cases are presented in Table 1. The results are in excellent agreement with the available solutions.

Table 1. Confirmatory results

Cases	Nusselt number: Known solution	Present solution	Percentage difference	Remarks
Case 1. $R_0/R_c = 0.2$	8.499 (Analytical)	8.471	0.33	Grid lines intersect orthogonally with the boundary
Case 2. $P/D = 1.6$	12.05 (Numerical)	11.95	0.83	Non-orthogonal intersection with the boundary
$P/D = 2.0$	15.26 (Numerical)	15.11	0.98	

Table 2. Predictions for single rod ring clusters

Sr No.	No. of rods	Rod radii	ϕ deg	b_1	d_h	Grid $N_r \times N_u$	$f \cdot Re$ Anal. [13]	$f \cdot Re$ This work	$u_{max}/\bar{u}$	$\bar{T}_f^*$	Nu	$T_{max}/\bar{T}_f$	Location of T_{max} θ deg	r
1	5	0.20	45.0	0.720	0.800	14 × 17	15.89	15.97	2.096	0.093	3.664	7.67	0.0	0.92
2	5	0.20	45.0	0.640	0.800	16 × 20	19.83	19.89	2.251	0.147	4.471	3.05	0.0	0.20
3	5	0.25	45.0	0.675	0.611	18 × 19	14.75	14.98	2.371	0.225	2.353	4.69	0.0	0.93
4	5	0.25	45.0	0.600	0.611	19 × 23	17.14	17.28	2.493	0.320	1.807	4.50	0.0	0.25
5	7	0.20	30.0	0.720	0.600	10 × 17	17.43	17.46	2.080	0.245	3.175	4.62	0.0	0.92
6	7	0.20	30.0	0.640	0.600	12 × 12	24.31	24.31	2.071	0.234	5.659	2.50	0.0	0.20
7	7	0.25	30.0	0.675	0.409	15 × 19	19.20	19.25	2.098	0.415	3.069	2.39	0.0	0.25
8	7	0.25	30.0	0.600	0.409	16 × 23	19.52	19.56	2.676	0.747	0.461	7.70	0.0	0.25
9	9	0.20	22.5	0.720	0.457	13 × 19	16.15	16.19	2.564	0.769	1.023	3.86	0.0	0.92
10	9	0.20	22.5	0.640	0.457	12 × 20	22.50	22.76	2.036	0.381	3.552	2.75	17.3	0.55
11	9	0.25	22.5	0.675	0.269	23 × 22	15.12	15.45	2.321	1.863	1.068	2.22	0.0	0.93
12	11	0.20	18.0	0.720	0.350	11 × 19	11.12	11.22	2.788	1.834	0.229	5.64	0.0	0.92

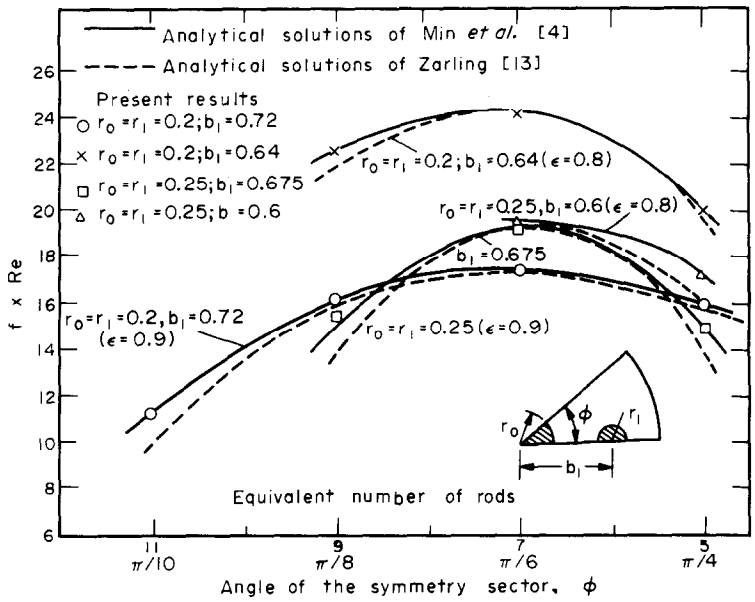

FIG. 4. $f \cdot Re$ variation with number of rods in a single rod ring cluster.

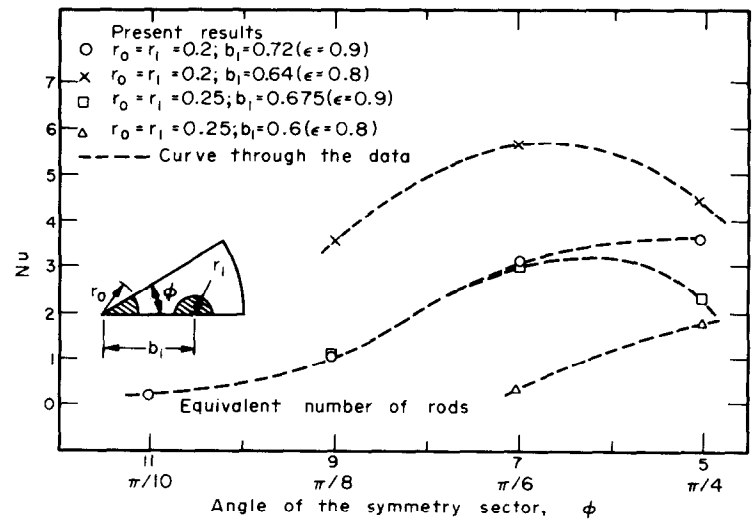

FIG. 5. Nu variation with number of rods in a single rod ring cluster.

3.3. *Single rod ring cluster results*

The predictions of $f \cdot Re$ as a function of the angle of symmetry sector ϕ (or the equivalent number of rods in the assembly) are plotted in Fig. 4 with rod radii and eccentricity ε defined by Min *et al.* [4] as parameters. The solutions obtained by Min *et al.* and Zarling [13] are shown for comparison. Results compare well with Zarling's data (see also Table 2). Substantial deviation is observed in Min *et al.*'s data for some geometries which could be due to the point matching technique used by them for satisfying the boundary conditions as pointed out by Zarling [13].

The Nu variation is shown in Fig. 5. The curves exhibit a similar trend as that of $f \cdot Re$ variation with the number of rods. The curves for $r_0 = r_1 = 0.2$; $b = 0.72$ and $r_0 = r_1 = 0.25$; $b = 0.675$ merge together beyond seven rods. This does not necessarily mean that the heat-transfer coefficients in the two cases are equal, because of the complicated geometrical factor, D_h involved in the definition of dimensionless temperature. The same is also the reason for unusually small magnitudes of Nu for certain geometrical conditions.

3.4. *19-Rod cluster results*

The effect of various geometrical parameters, viz. the wall spacing W, ϕ and the rod ring radii for 19-rod cluster with two rod rings is discussed below.

Effect of wall spacing W. The wall spacing W was varied by varying b_1 and b_2 ($b_2 = b_3$) such that ($b_2 - b_1$) was equal to 0.3. This configuration was chosen to facilitate comparison of the predictions with the calculations of Mottaghian and Wolf [7]. The effect of W on various characteristics is shown in Figs. 6–8. The $f \cdot Re$ results presented in Fig. 6 are compared with Mottaghian and Wolf's [7] results and found to be in good agreement. The $f \cdot Re$ product initially increases with W, reaches a maximum at $W = 0.35$ and then decreases continuously. Nu also varies in the same fashion as shown in the figure but its behaviour is more peakish than that of $f \cdot Re$ and its maximum occurs at $W = 0.3$. Average temperature of the rod surfaces, bulk mean temperature and their difference pass through a sharp minimum at $W = 0.3$ as seen from Fig. 7. The variation of average rod temperature for each rod and average channel wall temperature with W is plotted in Fig. 8. The central rod temperature is initially constant and increases sharply for $W > 0.3$ because of the influence of peripheral rods. The peripheral rod temperatures initially decrease as the influence of the channel wall reduces, pass through minima at $W = 0.3$ and increase beyond $W = 0.3$ due to the influence of the central rod and their influence on each other as they come closer. The channel wall temperature decreases as W increases and remains at nearly zero (which, incidentally implies that the channel wall temperature equals the minimum fluid temperature) beyond $W = 0.3$, indicating that there is no influence of rod temperatures on the channel wall.

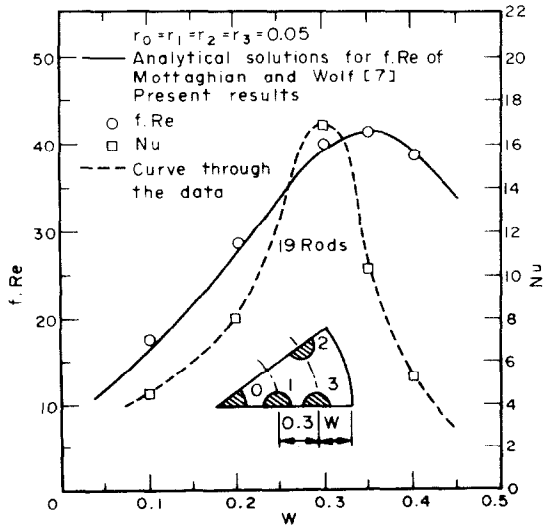

FIG. 6. $f \cdot Re$ and Nu as a function of wall spacing (W).

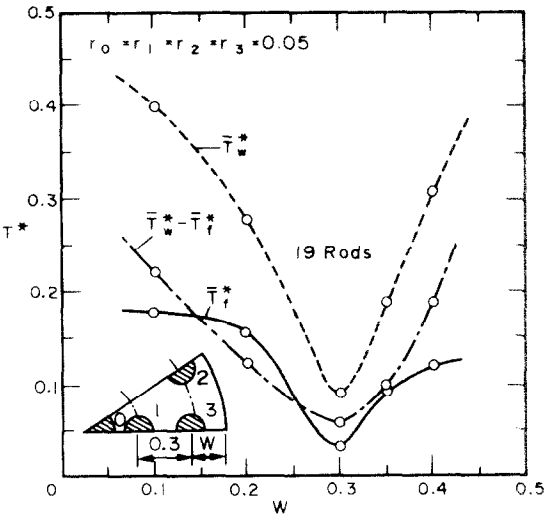

FIG. 7. Bulk mean temperature ($\bar{T}_f^*$), average temperature of the rod surfaces ($\bar{T}_w^*$) and their difference as a function of wall spacing (W).

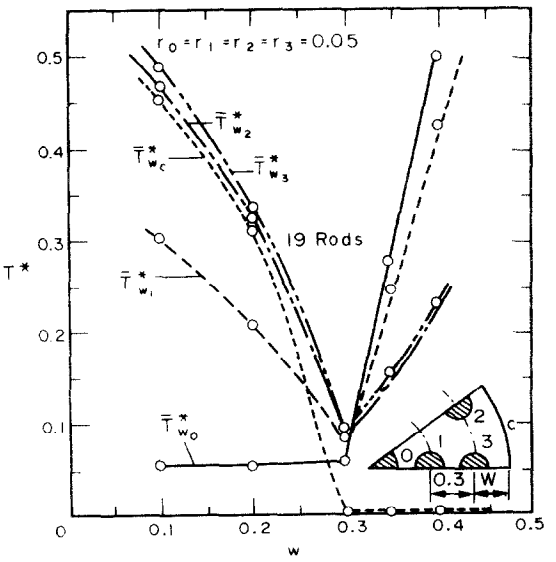

FIG. 8. Average rod and channel wall temperatures as a function of wall spacing (W).

The change in characteristics at $W = 0.3$ is attributed to the change in velocity profiles between the central rod and the peripheral rods and between the peripheral rods and the channel wall. The temperature profiles are of course governed by the velocity profiles. Velocity contours for three geometries with $W = 0.2$, 0.3 and 0.35 are shown in Fig. 9. For $W = 0.2$, the high velocity region lies in between the central rod and the first rod ring. The velocities are quite low in the vicinity of the second rod ring and the channel wall. This

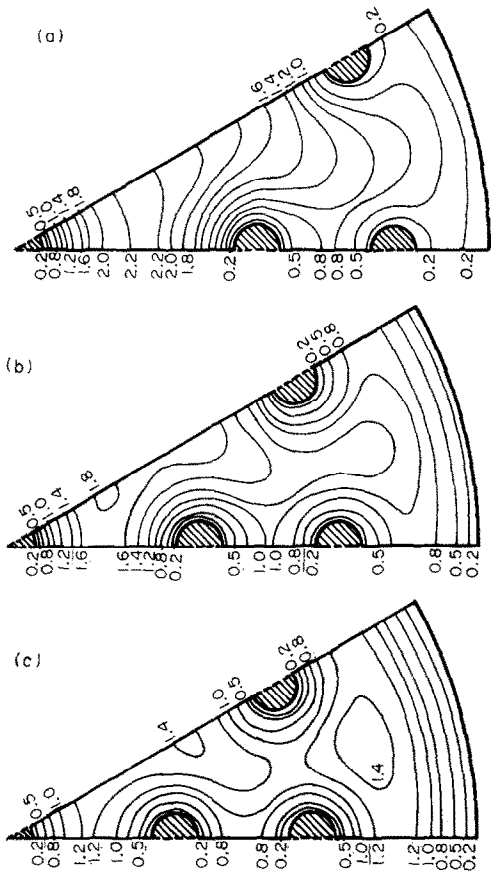

FIG. 9. Constant velocity ($u/\bar{u}$) contour lines for 19-rod cluster. $r_0 = r_1 = r_2 = r_3 = 0.05$; $b_3 = b_2$; $b_2 - b_1 = 0.3$: (a) $W = 0.2$; (b) $W = 0.3$; (c) $W = 0.35$.

results in relatively low temperature at the central rod and high temperatures at the peripheral rods and the channel wall. At $W = 0.3$, the high velocity zone spreads well beyond the second rod ring providing relatively substantial mass flow rates near all the solid walls. This leads to a comparatively favourable heat-transfer situation with low temperatures prevailing at all the surfaces. At $W = 0.35$ the high velocity zone passes beyond the second rod ring having a maximum cooling effect on the channel wall resulting in low channel wall temperature and high rod temperatures. The above discussion explains the sensitivity of the wall temperatures to the parameter W. It should be noted, however, that average wall temperatures have been plotted in Fig. 8 and the unusual sharpness in the curves at $W = 0.3$ is incidental.

Effect of rod radii for triangular array of rods. In order to facilitate comparison with Mottaghian and Wolf's [7] results a geometry was chosen such that distance P between the centres of rods 1, 2 and 3 shown in Fig. 10 was equal and thus forming a triangular array. The values of b_1, b_2, b_3 and P are same as those chosen by Mottaghian and Wolf.

In Fig. 10, on the X-axis are plotted the values of P/D instead of D. This is done to correspond with the manner of presentation adopted by Mottaghian

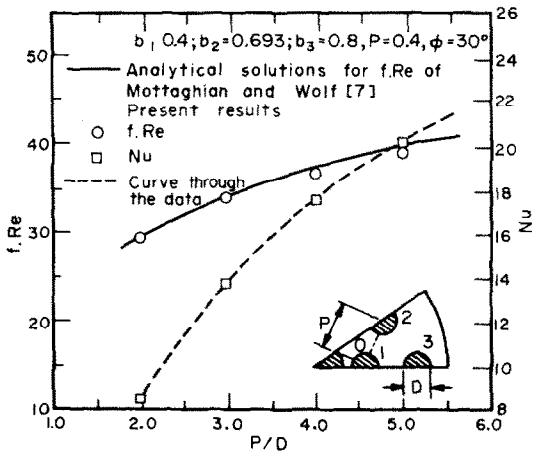

FIG. 10. $f \cdot Re$ and Nu variation with pitch-to-diameter ratio (P/D) in a 19-rod cluster with triangular array.

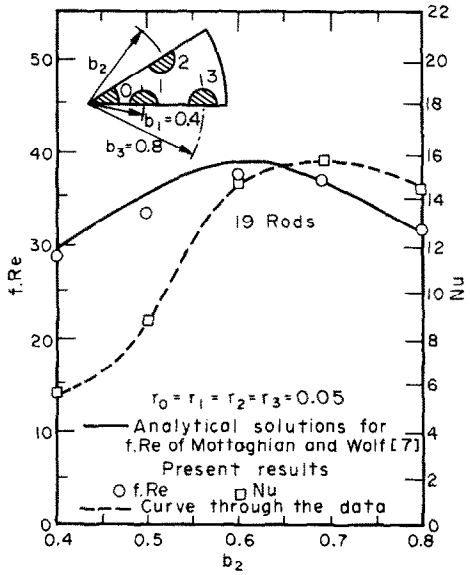

FIG. 11. $f \cdot Re$ and Nu variation with the radial displacement of the second rod ring with radius (b_2).

and Wolf. The $f \cdot Re$ results compare well with their solutions. $f \cdot Re$ and Nu monotonically increase with P/D. Similar variation is observed for an infinite triangular rod array as seen from the analytical solutions for $f \cdot Re$ of Sparrow and Loeffler [1] and from the predictions for Nu of Dwyer and Berry [3].

Effect of b_2. The effect of changing the second rod ring radius b_2 by keeping b_1 and b_3 fixed is presented in Fig. 11. The solutions (which have been tested for grid

Table 3. Predictions for multiple rod ring clusters

Sr No.	No. of rods	Rod radii	ϕ deg	b_1 b_2 b_3	d_h	Grid $N_r \times N_\theta$	$f \cdot Re$ Anal. [7]	$f \cdot Re$ This work	u_{max}/u	T_f^*	Nu	$T_{max} - T_f$	Location of T_{max} θ deg	r
1	19	0.0500	30.0	0.600 0.900 0.900	0.977	19 × 26	17.0	17.77	2.161	0.178	4.514	2.88	0.0	0.95
2	19	0.0500	30.0	0.500 0.800 0.800	0.977	19 × 26	28.0	28.80	2.273	0.153	8.111	2.33	0.0	0.85
3	19	0.0500	30.0	0.400 0.700 0.700	0.977	19 × 26	39.6	39.96	1.781	0.030	16.94	3.54	0.0	0.65
4	19	0.0500	30.0	0.350 0.650 0.650	0.977	19 × 26	41.5	41.24	1.518	0.094	10.39	2.95	0.0	0.05
5	19	0.0500	30.0	0.300 0.600 0.600	0.977	19 × 26	39.0	38.66	1.677	0.119	5.318	4.22	0.0	0.05
6	19	0.1000	30.0	0.400 0.693 0.800	0.559	23 × 26	29.8	29.45	1.601	0.215	8.655	2.14	0.0	0.10
7	19	0.0667	30.0	0.400 0.693 0.800	0.808	23 × 27	34.0	34.01	1.659	0.037	13.71	4.33	0.0	0.87
8	19	0.0500	30.0	0.400 0.693 0.800	0.977	23 × 26	36.8	36.80	1.687	0.032	17.60	3.64	2.0	0.84
9	19	0.0400	30.0	0.400 0.693 0.800	1.102	23 × 28	40.0	39.10	1.689	0.029	20.20	3.49	1.0	0.84
10	19	0.0500	30.0	0.400 0.600 0.800	0.977	19 × 29	38.8	37.31	1.598	0.068	14.67	2.44	6.0	0.37
11	19	0.0500	30.0	0.400 0.500 0.800	0.977	19 × 29	35.3	33.46	1.852	0.101	8.679	3.03	0.0	0.05
12	19	0.0500	30.0	0.400 0.400 0.800	0.977	19 × 26	29.8	28.67	1.997	0.108	5.569	4.19	0.0	0.05

independence) agree fairly well with Mottaghian and Wolf's [7] results for $b_2 > 0.6$, however, for $b_2 < 0.6$ the agreement with the analytical solutions is not entirely satisfactory. For the same flow area, $f \cdot Re$ increases with increasing ring radius b_2; reaches a maximum value at $b_2 = 0.63$ and then decreases with further increase in b_2. Therefore, from a pressure drop point of view it seems to be more advantageous to place additional rods into the first or third rod ring than to constitute a second rod ring.

The predicted Nu variation is also plotted in Fig. 11. Nu gradually increases with decrease in b_2, reaches a maximum value at $b_2 = 0.66$ and then decreases steeply with further decrease in b_2. Hence, from the point of view of heat transfer and pressure drop together, additional rods in the outermost ring seems to be optimum for the specified case.

3.5. *Effect of* ϕ

The effect of the angle of symmetry sector ϕ (or the equivalent number of rods in the assembly) is presented in Figs. 12 and 13. Rod radii are chosen as a parameter. The $f \cdot Re$ predictions are compared with the analytical solutions of Mottaghian and Wolf [7]. The analytical solutions deviate substantially from the present results as the rod radii and number of rods increase. The solutions obtained by the present method for 28 rod cluster with $r_0 = r_1 = r_2 = r_3 = 0.08$ differ by about 20% in spite of the grid independent solution obtained by increasing the grid lines from 11 × 28 to 20 × 28 (see Fig. 3).

Since (i) the results agree well with the analytical solutions for single rod ring array and for the cases shown in Figs. 6, 10, 11, (ii) the results are grid independent, and (iii) the boundary condition is satisfied at a sufficiently large number of points, the present solutions are believed to be correct.

The curves for Nu are presented in Fig. 12. Nusselt number decreases with the increase in rod diameters; however, the variation of $f \cdot Re$ and Nu are difficult to explain because of the complicated geometrical factor, D_h involved in the definitions of $f \cdot Re$ and T^*.

Table 3—*continued*

Sr No.	No. of rods	Rod radii	ϕ deg	b_1 b_2 b_3	d_h	Grid $N_r \times N_\theta$	$f \cdot Re$ Anal. [7]	$f \cdot Re$ This work	$u_{max}/\bar{u}$	$\overline{T}_f^*$	Nu	$T_{max}/\overline{T}_f$	Location of T_{max} θ deg	r
13	19	0.0500	30.0	0.400 0.800 0.800	0.977	19 × 26	31.0	31.57	1.879	0.040	14.45	3.95	0.0	0.85
14	19†	0.0500	30.0	0.400 0.800 0.800	0.977	20 × 26		31.48	1.915	0.040	14.43	3.89	15.0	0.85
15	19	0.0800	30.0	0.400 0.800 0.800	0.697	15 × 28	25.0	26.75	2.056	0.094	8.822	3.59	0.0	0.88
16	19†	0.0800	30.0	0.400 0.800 0.800	0.697	16 × 28		26.75	2.150	0.097	8.757	3.51	15.0	0.88
17	10	0.0500	60.0	0.400 0.800 0.800	1.300	23 × 26	26.0	26.07	1.937	0.028	14.73	4.48	0.0	0.85
18	28	0.0500	20.0	0.400 0.800 0.800	0.775	21 × 26	30.0	31.73	1.962	0.116	9.861	2.73	20.0	0.85
19	37	0.0500	15.0	0.400 0.800 0.800	0.637	16 × 26	25.5	27.81	2.102	0.251	5.836	2.40	15.0	0.85
20	46	0.0500	12.0	0.400 0.800 0.800	0.536	13 × 26	21.0	22.49	2.171	0.440	3.524	2.33	12.0	0.85
21	10	0.0800	60.0	0.400 0.800 0.800	1.040	20 × 28	22.5	22.40	2.037	0.051	8.956	4.53	0.0	0.88
22	28	0.0800	20.0	0.400 0.800 0.800	0.507	20 × 28	20.8	24.79	2.264	0.248	4.421	3.30	0.0	0.88
23	37	0.0800	15.0	0.400 0.800 0.800	0.385	16 × 28	14.7	17.94	2.293	0.789	1.734	2.84	15.0	0.88

†Doubly connected.

3.6. *Comment on data presented in the Tables 2 and 3*

Tables 2 and 3 present fluid flow and heat-transfer characteristics of single rod ring and multiple rod ring clusters respectively for 35 different configurations (in each case the grid was chosen in such a manner that the number of intersections at which the boundary conditions were satisfied were more than 70). The ratios $u_{max}/\bar{u}$ for these configurations vary between 1.6 and 2.8 which are normally found for noncircular ducts. The maximum temperature to bulk mean temperature ratios vary between 2.2 and 7.7. As expected, the maximum temperature always occurs on the rod surface where the gap between two solid walls is smallest. The tables also provide comparison of the presently predicted and previously analytically calculated results for $f \cdot Re$.

4. CONCLUSIONS

The following are the conclusions of the present paper:

(1) Heat transfer results for fully developed laminar flow in rod cluster assemblies of up to 46 rods have been obtained for the first time using the sector approach. Both singly, as well as doubly connected sectors have been considered.

(2) The predicted $f \cdot Re$ results are in excellent agreement with the analytical solutions for the majority of the cases. As the proximity between the rods increases the agreement between the present prediction and the analytical solutions of Mottaghian and Wolf [7] is poor. This conclusion points to the manner in which Mottaghian and Wolf have divided the region for the superposed solution and subsequently treated the boundary conditions. The present numerical solutions are, however, believed to be accurate in all cases.

(3) The predicted heat-transfer characteristics have shown plausible trends. The predictions have also brought out some unique features of the flow. For example, for a 19-rod cluster, it has been found that when $W = 0.3$, the characteristics exhibit a marked

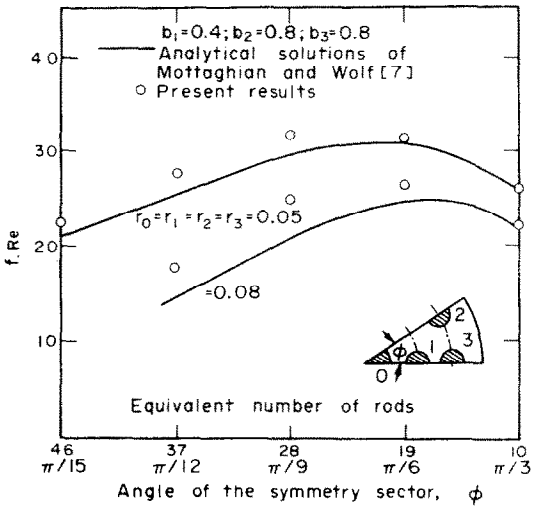

FIG. 12. $f \cdot Re$ variation with number of rods in a two rod ring cluster.

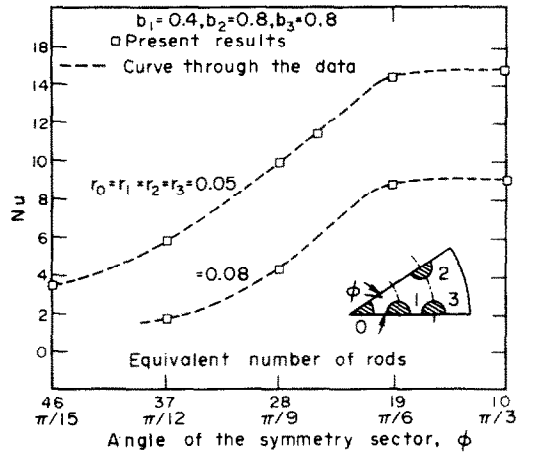

FIG. 13. *Nu* variation with number of rods in a two rod ring cluster.

change. Similarly it is also noticed that it is beneficial from both the pressure-drop and heat-transfer point of view to have only two rod rings in preference to three rod rings for 19-rod clusters.

(4) Fluid flow and heat-transfer characteristics over complex domains presented by symmetry sectors of rod clusters have been efficiently predicted with CPU times and storage not exceeding 1 min and 15 K on DEC system 10 computer.

Acknowledgement—The financial support provided for the present work by the Department of Atomic Energy, Government of India, under the project No. BRNS/Engg/5/74 is gratefully acknowledged.

REFERENCES

1. E. M. Sparrow and A. L. Loeffler, Jr., Longitudinal flow between cylinders arranged in a regular array, *A.I.Ch.E. Jl* **5**, 325–329 (1959).
2. E. M. Sparrow, A. L. Loeffler, Jr. and H. A. Hubbard, Heat transfer to longitudinal laminar flow between cylinders, *J. Heat Transfer* **83**, 415–422 (1961).
3. O. E. Dwyer and H. C. Berry, Laminar flow heat transfer for in-line flow through unbaffled rod bundles, *Nucl. Sci. Engng* **42**, 81–88 (1970).
4. T. C. Min, H. W. Hoffman, T. C. Tucker and F. N. Peebles, An analysis of axial flow through a circular channel containing rod cluster, *Dev. Theoret. Appl. Mech.* **3**, 667–690 (1966).
5. R. A. Axford, Summary of theoretical aspects of heat transfer performance in clustered rod geometries, in *Heat Transfer in Rod Bundles*, pp. 70–103. ASME, New York (1968).
6. J. P. Zarling, Laminar-flow pressure drop in symmetrical finite rod bundle, *Nucl. Sci. Engng* **61**(2), 282–285 (1976).
7. R. Mottaghian and L. Wolf, A two-dimensional analysis of laminar fluid flow in rod bundles of arbitrary arrangement, *Int. J. Heat Mass Transfer* **17**, 1121–1128 (1974).
8. D. I. Gunn and C. W. Darling, Fluid flow and energy losses in non-circular conduits, *Trans. Instn Chem. Engrs* **41**, 163–173 (1963).
9. K. Rehme, Laminarstromung in stabbündeln, *Chemie-Ingr-Tech.* **43**, 962–966 (1971).
10. D. W. Peaceman and H. H. Rachford, Jr., The numerical solution of parabolic and elliptic differential equations, *J. Soc. Ind. Appl. Math.* **3**(1), 28–41 (1955).
11. D. Greenspan, *Introductory Numerical Analysis of Elliptic Boundary Value Problems*, pp. 39–42. Harper, New York (1965).
12. W. M. Kays, *Convective Heat and Mass Transfer*, p. 114. McGraw-Hill, New York (1966).
13. J. P. Zarling, Personal Communication (16 December 1976).
14. B. Carnahan, H. A. Luther and J. O. Wilkes, *Applied Numerical Methods*, p. 463. John Wiley, New York (1969).
15. R. W. Benodekar and A. W. Date, Finite difference procedure for solution of Poisson equation over complex domains with Neumann boundary conditions, *J. Comput. Fluids*, to be published.

PREDICTION NUMERIQUE DES CARACTERISTIQUES DE TRANSFERT THERMIQUE D'UN ECOULEMENT LAMINAIRE PLEINEMENT DEVELOPPE DANS UN CANAL CIRCULAIRE CONTENANT UNE GRAPPE DE TUBES

Résumé—On présente les résultats de calcul pour un écoulement laminaire pleinement développé dans des assemblages de grappes de tubes. Le problème est résolu par une méthode de différences finies utilisant une approche sectorielle où le plus petit segment de symétrie de la grappe est considéré comme la caractéristique de la section de passage. La perte de charge est rapportée au nombre de Reynolds de frottement et elle est comparée aux résultats donnés dans la bibliographie. Les nombres de Nusselt sont présentés pour plusieurs configurations. Les résultats sont exprimés en fonction de l'espacement des parois du canal, du déplacement radial des anneaux des tubes, du nombre de tubes dans l'assemblage et du diamètre des tubes.

DIE NUMERISCHE BESTIMMUNG DER WÄRMEÜBERTRAGUNGSCHARAKTERISTIK EINER VOLL AUSGEBILDETEN LAMINARSTRÖMUNG DURCH EINEN RUNDEN KANAL MIT STABBÜNDELN

Zusammenfassung—Dieser Bericht beschreibt die Ergebnisse der Berechnung einer vol ausgebildeten Laminarströmung zwischen Stabbündelanordnungen. Die Aufgabe wird durch eine finite Differenzenmethode gelöst, bei der eine abschnittsweise Näherung angewandt wird, wobei die kleinste Symmetrieeinheit des Bündels als kleinstes charakteristisches Strömungsgebiet betrachtet wird. Die Druckabfallcharakteristika werden in Abhängigkeit von den Produkten aus Reibungskoeffizient und Reynolds–Zahl dargestellt und werden mit den in der Literatur verfügbaren Werten verglichen. Die Nusselt–Zahlen werden für verschiedene Anordnungen aufgeführt. Die Ergebnisse werden ausgedrückt in Abhängigkeit des Kanaldurchmessers, der radialen Versetzung der Stäbe, der Anzahl der Stäbe innerhalb des Bündels und des Durchmessers der Stäbe.

ЧИСЛЕННЫЙ РАСЧЕТ ХАРАКТЕРИСТИК ТЕПЛООБМЕНА ПРИ ПОЛНОСТЬЮ РАЗВИТОМ ЛАМИНАРНОМ ТЕЧЕНИИ В КРУГЛЫХ КАНАЛАХ, СОДЕРЖАЩИХ ПУЧКИ СТЕРЖНЕЙ

Аннотация — В статье представлены результаты расчетов для полностью развитого ламинарного обтекания пучков стержней. Задача решается методом конечных разностей путем разбиения всего канала на секторы, где только отрезок наименьшей симметрии пучка нужно принимать за характерную область течения. Перепад давления выражается через произведение коэффициента трения на число Рейнольдса и сравнивается с опубликованными данными. Для нескольких конфигураций приводятся значения числа Нуссельта. Результаты представлены как функции расстояния между стенками канала, радиальных смещений пучков, числа стержней в пучке и диаметра стержней.